Homoepitaxial Diamond Grown in a Liquid Metal Solvent

Yan Gong[1,2], Da Luo[1*], Myeonggi Choe[1,3], Chohee Hyun[5], Chunhui Wang[1], Meihui Wang[1], Won Kyung Seong[1], Tae Joo Shin[5,6], Zonghoon Lee[1,3], Da Zhan[7], Rodney S. Ruoff[1,2,3,4*]

Affiliations:

[1]Center for Multidimensional Carbon Materials (CMCM of the Institute for Basic Science), Ulsan 44919, Republic of Korea

[2]Department of Chemistry, Ulsan National Institute of Science and Technology (UNIST), Ulsan 44919, Republic of Korea

[3]Department of Materials Science and Engineering, Ulsan National Institute of Science and Technology (UNIST), Ulsan 44919, Republic of Korea

[4]School of Energy and Chemical Engineering, Ulsan National Institute of Science and Technology (UNIST), Ulsan 44919, Republic of Korea

[5]UNIST Central Research Facilities (UCRF), Ulsan National University of Science and Technology (UNIST), Ulsan 44919, Republic of Korea

[6] Graduate School of Semiconductor Materials and Devices Engineering, Ulsan National University of Science and Technology (UNIST), Ulsan 44919, Republic of Korea

[7]State Key Laboratory of Luminescence and Applications, Changchun Institute of Optics, Fine Mechanics and Physics, Chinese Academy of Sciences, Changchun 130033, China

*Correspondence to: rsruoff@ibs.re.kr, ruofflab@gmail.com (R.S.R.); luodarhoda@gmail.com (D.L.)

Abstract

A single-crystal diamond substrate (SCDS) with a (100) surface orientation was submerged in liquid gallium containing a small amount of dissolved silicon, and exposed to a mixture of methane and hydrogen at 1 atm and 900 ºC. New growth diamonds were found that are single crystal square pyramids with (111) facets and that are homoepitaxial to the substrate, as proven by scanning and transmission electron microscopy, and small angle X-ray scattering and diffraction. Raman spectroscopy with ^{13}C-labeling prove that the methane as well as the SCDS are the carbon source for the newly grown diamond. This approach opens up new ways for growing diamond in liquid metal systems.

Main Text:

Introduction:

There are two conventional ways of growing synthetic diamond of moderate size (centimeter and larger scale), and both can yield either polycrystalline or single crystal diamond. High pressure and high temperature ("HPHT") growth in the presence of metal catalyst(s) can now yield single crystal diamonds as large as one cubic centimeter [1], and chemical vapor deposition (CVD), such as hot wire CVD but particularly plasma-enhanced CVD (PE-CVD) can deposit large area single crystal diamond [2], as well as polycrystalline diamond. Very large single crystal "bias-enhanced" CVD epitaxial diamond films have also been recently achieved[3]. The growth of synthetic diamonds has been extensively reviewed [4], and the properties of diamond [5] and various applications of synthetic (and natural) diamonds have been described at length in many reviews, a few of which are cited here [1,6,7]. A third way of making synthetic diamond is by the "detonation method", in which "nanodiamonds" can be generated in ton quantity even in a single run and their synthesis

and properties have been reviewed [8]. Nanodiamonds are used in biomedical applications[9].

Diamond is the hardest known material, has the highest atomic density, the highest thermal conductivity, a large band gap, and when doped with N or Si has vacancy centers that are of interest for extremely sensitive magnetic sensing [10] and for use as "Q-bits" such as in quantum computers [11,12]. Diamond has a large number of already realized or potential applications, and shows great promise for very high power electronics [13].

We have discovered a method to grow diamond that we describe in detail below. We find that it can be grown with homoepitaxy on single crystal diamond substrates with a (100) surface orientation that are submerged in liquid metal, specifically liquid gallium. Our vapor-liquid-solid (VLS) growth of diamond involves exposing the liquid gallium containing a small amount of deliberately added silicon to a mixture of methane and hydrogen gas at 760 Torr and 900 ºC for several hours. The new diamond grows as square pyramids that are epitaxial to the (100) single crystal diamond substrate on which they grow and that have four (111) facets. Spectroscopy, scanning and transmission electron microscopy, and small angle X-ray scattering and diffraction, as described in detail below, unambiguously prove that the new diamond is single crystal, homoepitaxial.

Our growth of diamond on diamond-substrates submerged in liquid gallium at room pressure and modest temperature suggests that a variety of liquid metals are likely to act as solvents and perhaps as catalysts (indium, tin, lead, mercury, bismuth, others) as well, and the role of silicon and hydrogen will be intensely studied and eventually understood in detail. Many other elements can be added to such low temperature liquid metals and we suggest this is likely to result in new methods of synthesizing diamond particles by homogeneous nucleation and growth in the liquid metal, or to accelerate and advance the growth on a variety of surfaces, not only diamond but

others such as sapphire, silicon carbide, quartz, or diamond or other particles in the liquid metal. It seems likely that solid carbon can also act as a precursor, particularly when one considers that the growth of graphene using liquid gallium or liquid tin has been reported from solid carbon as well as gaseous precursors and on a variety of substrates [14-16].

Results and Discussion

We describe here a new way to grow diamond based on a vapor-liquid-solid (VLS) method. The *vapor* is a mixture of methane and hydrogen gases, the *liquid* is gallium with a small amount of dissolved silicon, and the *solid* is single crystal diamond with surface orientation (100), referred to as single crystal diamond substrate (SCDS-100). The volume ratio of methane and hydrogen (referred to as CH_4/H_2; we note that this is very close to the ratio of partial pressures as well), temperature of the liquid Ga with small amounts of added Si, exposure time to CH_4 and H_2, and the concentration of silicon in the liquid gallium, were growth parameters that were varied; the pressure was always held at about 760 Torr.

A schematic of the configuration we used is shown in Figs. 1A and 1B with a photograph in Fig. 1C. Here we describe the conditions that favored new diamond growth at the SCDS-100 surface. The quartz tube furnace was heated to 900 ºC and held at that temperature; CH_4 and H_2 were then introduced at a 1/100 ratio until a pressure of 760 Torr was reached, and the gases were then shut off for the static pressure growth runs. A crucible contained the diamond substrate submerged in liquid gallium with 0.57 at % of dissolved silicon. The growth of new diamond was found to be quite sensitive to the amount of Si in the liquid gallium. Figs. 1E, 1F, and 1G show scanning electron microscopy (SEM) images of new growth diamond (NGD) and some regions where silicon carbide grew on the SCDS-100 (Fig. 1E). The NGD consists of square pyramids that

are epitaxial to the (100) surface and have (111) sides. With this growth condition a high density of diamond pyramids was achieved and silicon carbide particles were typically found in between regions having a relatively dense number of diamond pyramids. The pyramids were always well aligned with each other (Figs. 1F and G) and the pyramid apex was clearly seen by tilting the sample 60.0 degrees, as shown in Fig. 1H.

Raman spectra were acquired from the as-received SCDS-100 and from the "new growth diamond" (NGD) obtained using $^{13}CH_4$. The molecular purity of our as-received ^{13}C-labeled methane is 99 %. Fig. 2A shows the strong Raman peak of as-received SCDS at 1333cm^{-1}, while Fig. 2B and Fig. 2C show the Raman spectra of ^{13}C-NGD after $^{13}CH_4$ was used for the growth. We found certain regions show pure ^{13}C-labeled diamond, while certain regions contained a mixture of ^{13}C-labeled diamond and ^{12}C diamond. Furthermore, some regions only contained ^{12}C diamond. Fig. 2B shows the ^{13}C-NGD Raman peak at 1282cm^{-1} along with the 1333cm^{-1} Raman peak [17]. The expected frequency blue shift for 100 % ^{13}C-labeled diamond is 51 cm^{-1}, i.e., from 1333 to 1282 cm^{-1} and this was observed in certain regions. Other regions showed the NGD Raman peak at 1295cm^{-1} (38cm^{-1} blue shift), 1299cm^{-1} (34cm^{-1} blue shift) and 1305cm^{-1} (27cm^{-1} blue shift) along with the 1333cm^{-1} Raman peak, respectively (Fig. 2C). These blue shifts indicated the concentration of ^{13}C in those regions are 71.7%, 64.2%, and 50.9%, respectively. It suggested the carbon source of NGD is from CH_4 as well as from the SCDS.

We used SEM images acquired at different sample orientations, and cross-sectional TEM, to study the geometry and atomic-scale structure of the new growth pyramids.

Cross-section TEM samples prepared by FIB showed pyramids, silicon carbide, and a few microns (about 5 μm) of the SCDS-100 in the FIB prepared regions near the regions imaged by TEM (which are about 100 nm thick). A typical cross-section TEM image of a new growth pyramid

is shown in Fig. 3A Electron energy loss spectroscopy (EELS) was used to characterize the new growth pyramid as well as the substrate. The standard typical diamond EEL spectrum was used for comparison. The EEL spectra of pyramids and substrate both match the reported EEL spectrum of diamond, confirming that the new growth pyramid is diamond (Fig. 3B).

Atomic resolution TEM (AR-TEM) images were obtained from the region indicated by the red dotted square inset in Fig. 3C, which shows a high magnification image of the region indicated by the green square in (A) that shows that the new growth pyramid atomic structure perfectly matched that of the reported diamond atomic structure (Fig. 3D). Also, the fact that the pyramid grows homoepitaxially from the (100) substrate is confirmed by the following two observations. (i) A selected area electron diffraction (SAED) pattern from the entire area of (A) is shown as Fig. 3E and contains only one single crystal diamond pattern; (ii) Fig. 3C shows the Fast Fourier Transform (FFT) patterns from an image of the new growth pyramid as well as of the substrate. The inset red dotted square shows the new growth pyramid FFT pattern, and the inset blue dotted square shows the substrate FFT pattern, with the two patterns matching perfectly. The diamond pyramids thus show homoepitaxy on the SCDS-100. TEM Energy-dispersive X-ray spectroscopy (EDX) mapping of a new growth pyramid, Fig. 3F, shows it to be pure C. The sample was coated with Ti to make it electrically conductive and to protect the pyramids from FIB-induced damage.

Synchrotron GI-SAXS measurements were performed to obtain statistically averaged information (complementary to the SEM results) about the shape, faceting and orientation of the diamond pyramids on the SCDS-100. We studied two kinds of samples, "NGD-1" which contained only diamond pyramids on SCDS-100 (growth conditions: 760 Torr and 900 ºC for 12h with 0.57 at % Si in gallium, CH_4/H_2 is1/100); we removed silicon carbide from NGD-1 by scraping it off. "NGD-2" contained both silicon carbide and pyramidal diamonds (growth

conditions: 760 Torr and 900 ºC for 12h with 0.62 at % Si in gallium, CH_4/H_2 is 1/100). The GI-SAXS pattern showed very strong facet streaks for every 90º azimuth (Ω, the rotation angle of the sample around the surface normal) in turn (Ω = 0º, 90º, 180º and 270º), suggesting square pyramid diamond growths of NGD-1 because the facet streak in the GI-SAXS pattern is observed when the beam is parallel to the facet or particle edge (*18*). The schematic GI-SAXS experimental set-up and representative 2D GI-SAXS patterns measured and simulated at Ω = 0º and 45º are shown in Fig. 4. The synchrotron X-ray beam irradiates the NGD on SCDS-100 at a grazing angle α_i = 0.08º ~ 0.22º, during which the sample is rotated around the surface normal over the range Ω = 0º to 360º (Figs. S9 and S10). When the azimuthal angle is 0º, the GI-SAXS pattern has distinct facet streaks (scattering rods) at -54.4º and 55.1º with respect to the surface normal, which correspond to the {111} facets of a cubic structure. In the case of Ω = 45º, the GI-SAXS pattern shows very weak and diffuse streaks at 45º with respect to the surface normal, indicative of scattering from the edges of the square base pyramids. The measured and simulated GI-SAXS results in Fig. 4 are in good agreement.

The facet orientation of the square pyramids on the SCDS-100 was further studied by SEM imaging at tilt angles from 10.0º to 40.0º. The apex is projected at different positions when different tilt angles are used for imaging, and by measuring the position of the apex, one can obtain the intersection angle between the face and the base of a square pyramid. Without tilting, the apex of the pyramid is located at the center of the square base (see Fig. 4G). For a tilt of 35.0º, the apex of the pyramid just overlapped an edge of the square base (see Fig. 4H). A series of tilt images shows that the angle between the faces of the pyramid and square base is very close to 55.0º (for a perfect join of (100) with (111) facets, an angle of 54.7º is expected). Because the surface orientation of the SCDS is (100) the 4 faces of the pyramids have a {111} orientation.

To study whether growth continues after pyramids have "achieved" four full (111) faces, we did a sequential growth study, and measured the diagonals of the square pyramid bases as a function of time. The size distributions obtained strongly suggest that growth continues on the (111) facets as the pyramids become larger and larger (Fig. 5).

The kinetics of growth of NGD was further studied (Fig. 6). The growth rate of NGD was calculated by dividing the side length of the square base of the pyramid diamond by the growth time. We found the growth rate at 880 °C is 1.56±0.20 nm/h, that is increased to 4.70±0.59 nm/h at 930 °C and is further increased to 20.0±10.0 nm/h at 980 °C. The growth rates were then plotted in Fig. 6D as a fit to the Arrhenius equation, and an activation enthalpy of 3.40 eV (328 kJ/mol) was obtained.

We also found there are crystals formed on the apex regions of some pyramid diamonds (Fig. 7A). These crystals and the pyramid diamonds are aligned along <110> directions of the SCDS-100 surface. EDX spectra collected from such crystal regions shows the presence of Si in the structure (Fig. 7B). We did cross-section STEM imaging and also found a pyramid diamond with a crystal at the apex. The uniform contrast of both regions in the STEM image suggests that both are single crystals (Fig. 7C). EDX maps of the crystal region show uniform distribution of both Si and C in its structure (Fig. 7D). AR-TEM image shows that the lattice parameter of the crystal is matched with the structure of 3C-SiC (Fig. 7E), and the lattice of the 3C-SiC crystal was found to be aligned with the lattice of the underlying pyramid diamond, suggesting an epitaxial relationship between the two structures. (We imaged the interface between another 3C-SiC crystal and a pyramid diamond and also found this epitaxy between the two structures). We note this epitaxial relationship explains the alignment between the 3C-SiC crystals and the pyramid diamonds as shown in SEM imaging (Fig. 7A). Such a 3C-SiC crystal is likely to play important

role in the growth of pyramid diamonds, including perhaps in the nucleation of the pyramid diamond. The 3C-SiC crystals might either grow into bigger sizes or are perhaps “etched” into smaller sizes during the growth of the pyramid diamonds, due to the fact that i) the 3C-SiC crystals are in different sizes (e.g., Fig. 6B-C and 7A), and ii) some apex regions do not show the presence of 3C-SiC crystals (e.g., Fig. 3A, 6B-C and 7A).

In our study we have used a gas phase precursor, methane. It can be expected that solid carbon or other solid precursors containing carbon that are mixed directly into the liquid metal will also yield new diamond.

In summary, considering the large number of possibilities for low melting point “liquid metals”, their eutectics, and the possibility of adding different amounts of various other elements that can act as catalysts (simply as one example among many, such as dissolving some nickel in gallium or bismuth), the possibilities for exploring diamond growth as a result of our discovery are exceptionally promising.

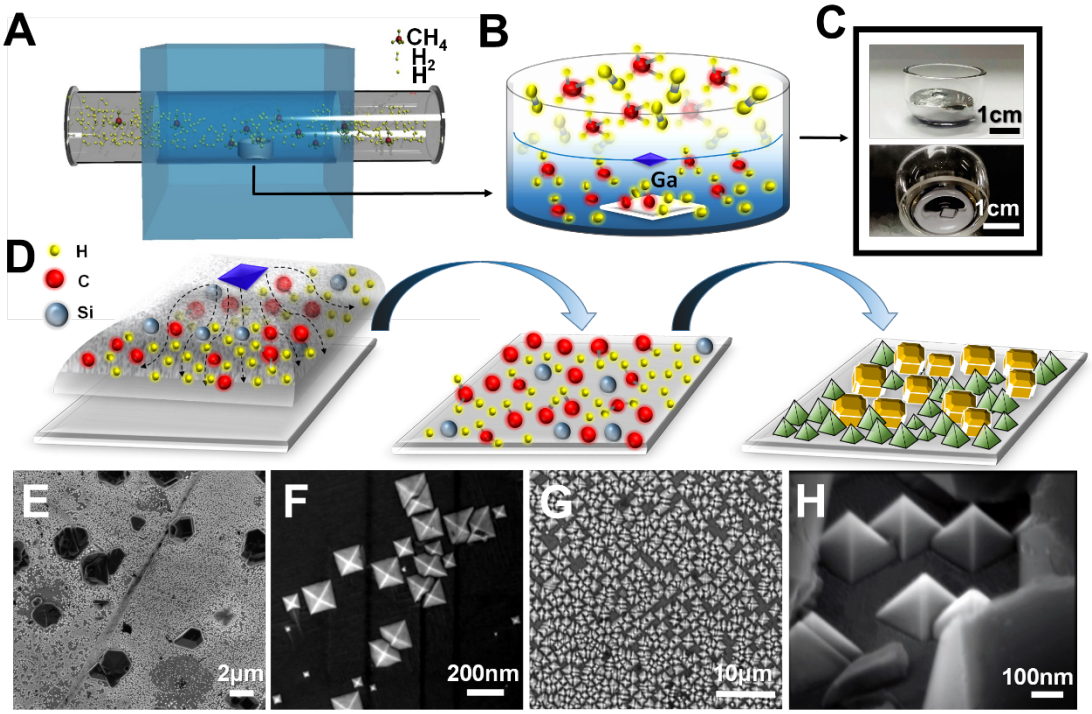

Figure. 1. (A) Schematic of the quartz tube furnace with the crucible inserted. (B) Schematic of the crucible containing liquid gallium, the diamond substrate, and silicon dissolved. (C) Side view photo (above) and bottom view photo (below) of the crucible configuration. (D) Schematic of new diamond growth. (E) Low magnification SEM image. The lighter regions contain many diamond pyramids and the darker regions are composed of silicon carbide particles on the SCDS. (F) High magnification SEM image of diamond pyramids grown on the (100) SCDS. (G) A region containing only diamond pyramids that are epitaxial to the (100) SCDS. (H) A high magnification SEM image of a region containing both diamond pyramids and silicon carbide particles surrounding them. The sample was tilted 60.0°.

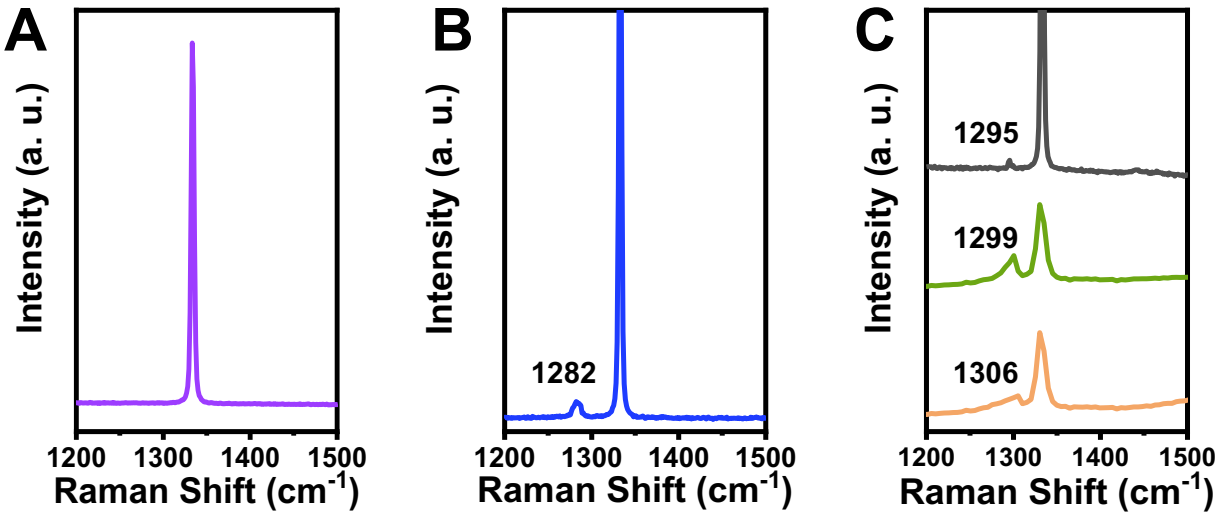

Figure. 2. Raman spectra of as-received SCDS and ^{13}C-labeled NGD on the SCDS. (A) Raman spectrum of the as-received SCDS. (B) Raman spectrum of ^{13}C-labeled NGD on the SCDS, that shows the ^{13}C-labeled diamond peak at 1282 cm^{-1} as well as the large peak at 1333 cm^{-1} from the underlying SCDS. (C) Raman spectra of ^{13}C-labeled NGD on the SCDS in different regions that show the ^{13}C-labeled diamond peak at 1295 cm^{-1}, 1299cm^{-1}, 1306cm^{-1}, respectively. The large peak at 1333 cm^{-1} is from the underlying SCDS.

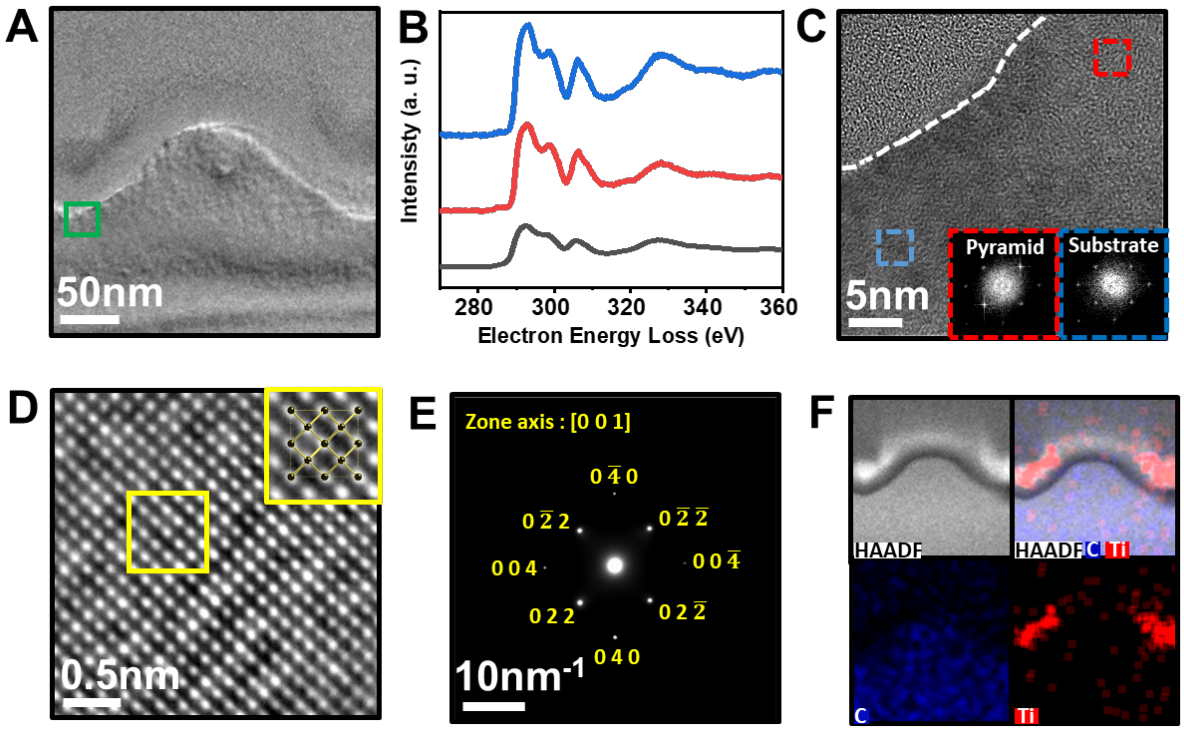

Figure 3. Homoepitaxial new growth pyramid diamond on SCDS. (A) Cross-section TEM image of a new growth pyramid. (B) EEL spectra of the pyramid, substrate and typical diamond. (C) High magnification image of the region indicated by the green square in (A). Insets are the FFT patterns from the pyramid and substrate. (D) AR-TEM image of the region indicated by the red dotted line square of (C). Inset shows the atomic structure of the pyramid. (E) SAED pattern from the entire area of (A). (F) EDX mapping of (A).

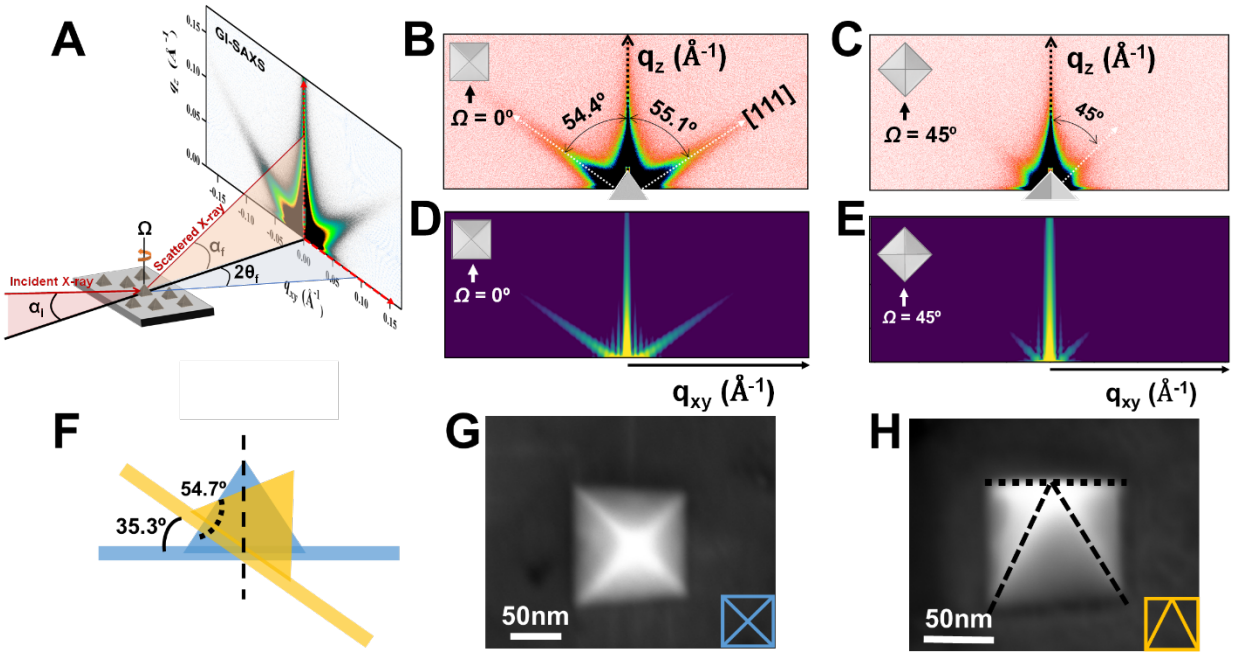

Figure 4. GI-SAXS experimental set-up and GI-SAXS patterns. (A) Illustration of the GI-SAXS experimental geometry. (B and C) experimental GI-SAXS patterns measured at azimuthal angles of Ω = 0º and 45º, respectively. (D and E) simulated GI-SAXS patterns of square base pyramids with 100 nm base side length and 70.7 nm height (slant angle of pyramid = 54.74º) at Ω = 0º and 45º, respectively. (F) Diagram of tilting sample 35.0º. (G) SEM image of pyramid without tilt. (H) Sample was tilted 35.0º.

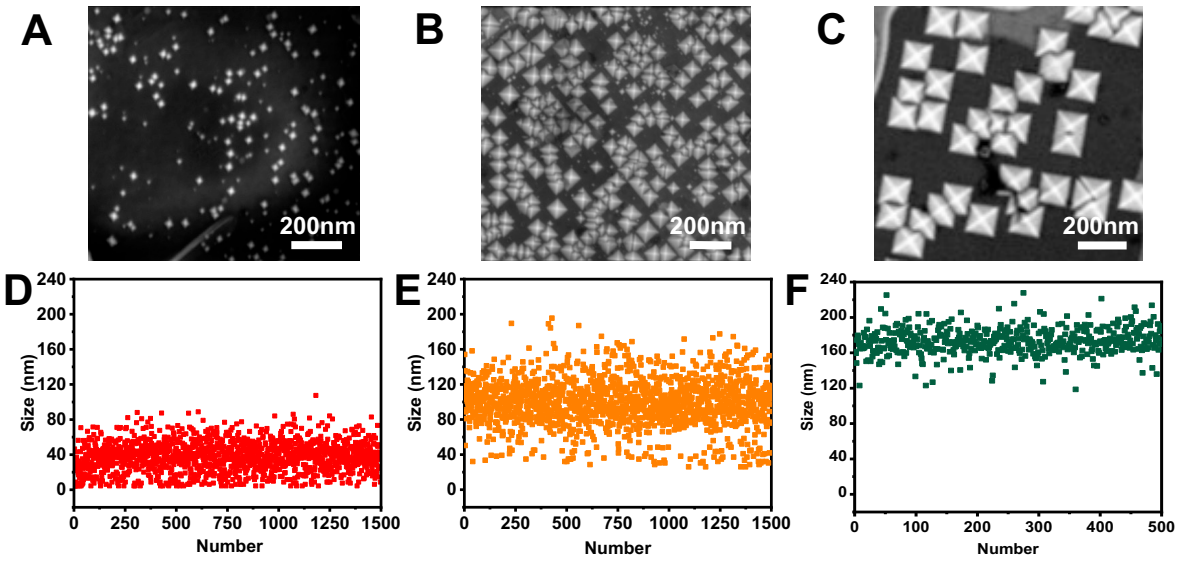

Figure 5. Sequential growth. SEM images of NGD growth after different times. The sample was prepared by annealing SCDS-100 in liquid 0.57 at % Si in Ga at 900 ºC, ratio of partial pressures CH_4/H_2 was 1/100 and pressure 760 Torr. (A to C) SEM images of (A) NGD grown for 6h, (B) sample A after a further 12h growth and (C) sample B after a further 20 h growth. (D to F) Respective size distributions of the islands in (A to C) measured using the diagonals of the square pyramids. The mean diagonals are respectively around 40, 100, and 170 nm. In sample C some of the pyramids have merged, as shown in the inset in F; we note that we considered only the isolated pyramids for obtaining the size distributions.

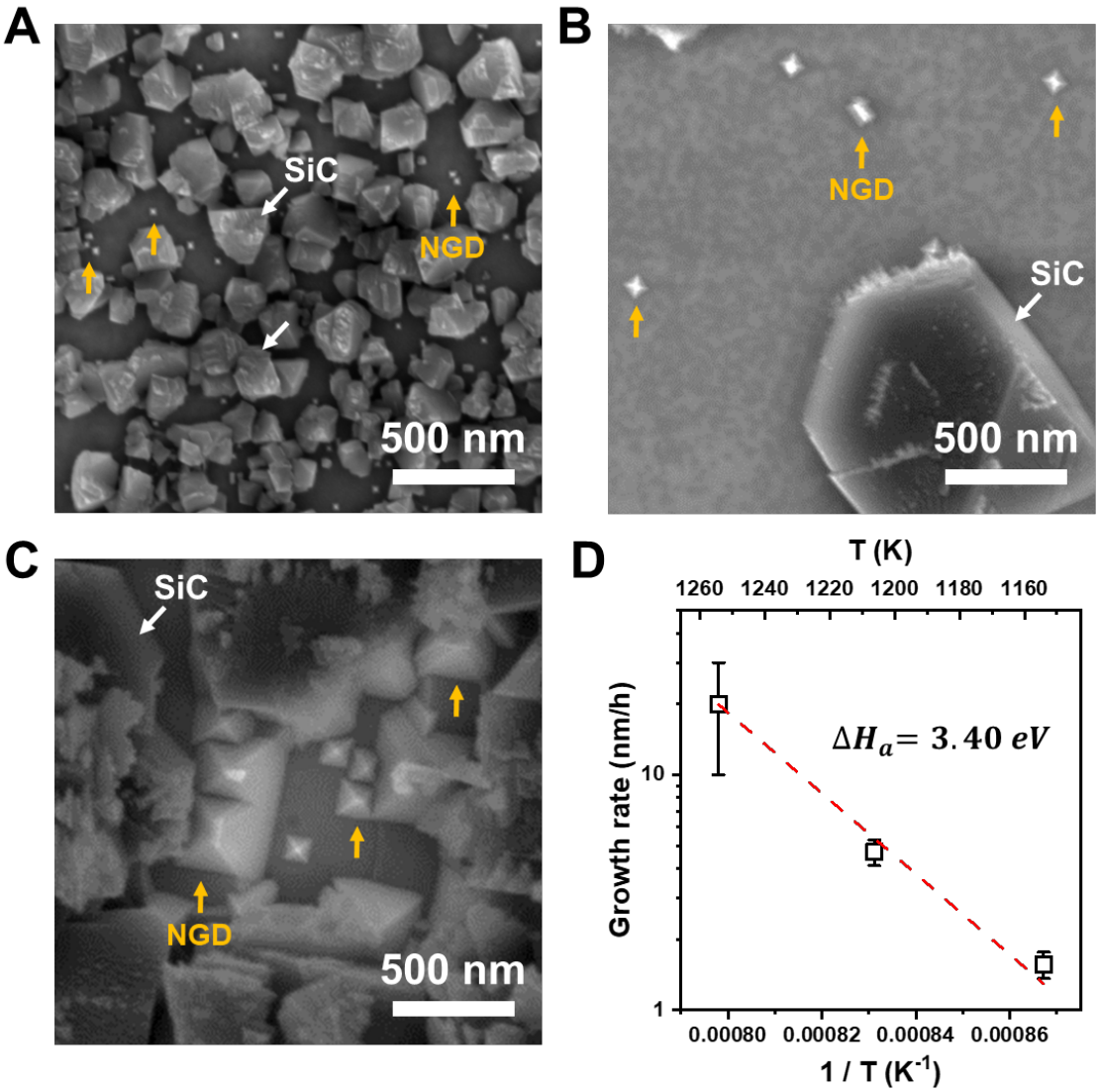

Figure 6. Kinetics of pyramid diamonds grown on SCDS-100. (A-C) Typical SEM images of NGD after growth (A) at 880 °C for 15 h, (B) at 930 °C for 17 h, and (C) 980 °C for 15 h. (D) Arrhenius plot of the growth rate of NGD.

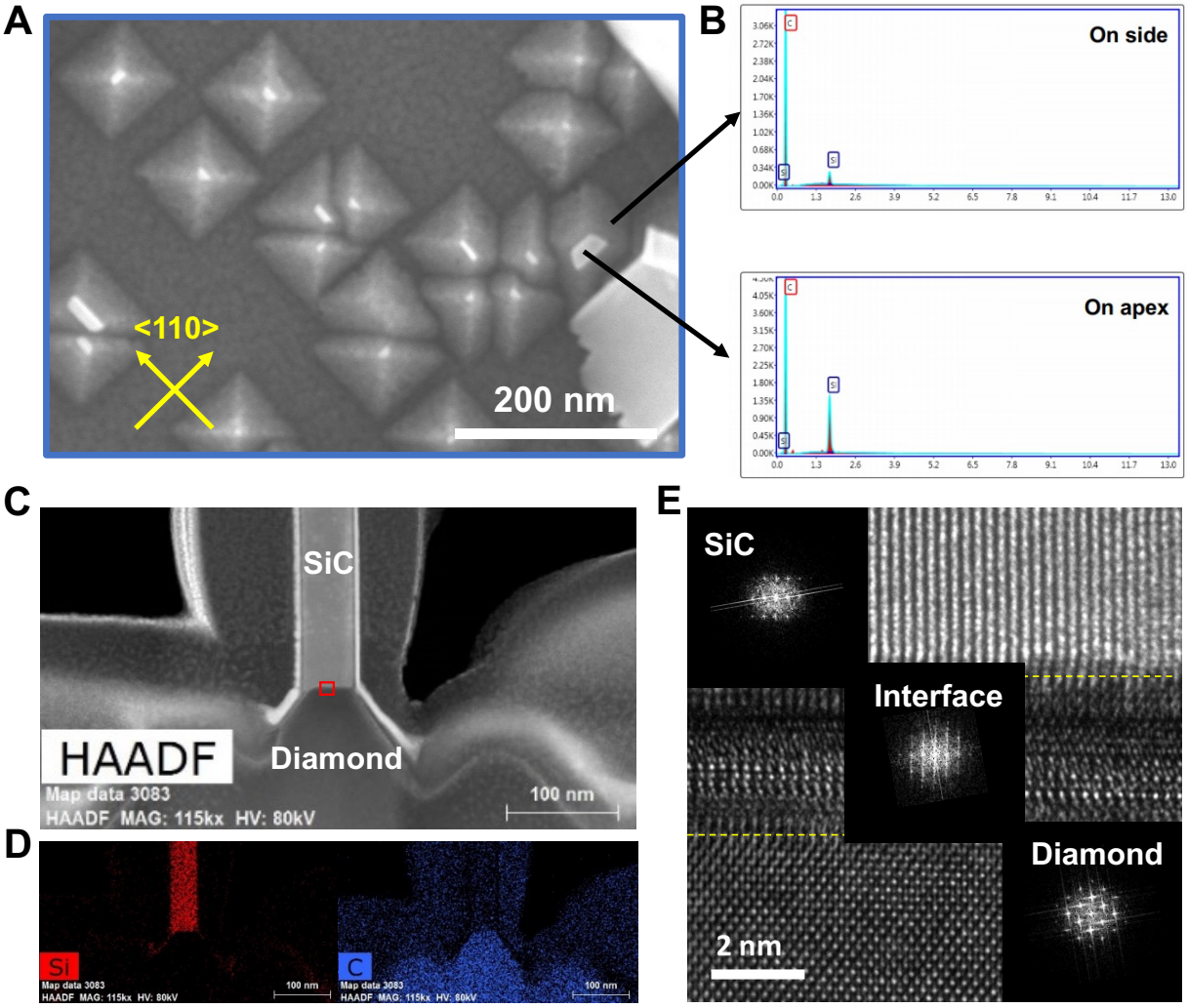

Figure 7. 3C-SiC crystals on apex of pyramid diamonds. (A) SEM image of NGD grown on SCDS-100 showing 3C-SiC crystals on the apex. (B) SEM EDX spectra collected from the side and the apex regions. (C) Cross-section STEM image of a pyramid diamond with a 3C-SiC crystal at the apex region. (D) EDX maps of (C) showing the presence of Si and C. (E) AR-TEM image of the red square region marked in (C) with FFT patterns converted from different regions.

References

1. Tatje, R., Diamond-The Ultimate Gemstone. GEMMOLOGICAL ASSOC GREAT BRITAIN 21 ELY PLACE, LONDON, EC1N 6TD, ENGLAND: 2017.
2. Teii, K., Plasma Deposition of Diamond at Low Pressures: A Review. *IEEE Transactions on Plasma Science* **2014,** *42* (12), 3862-3869.
3. Yaita, J.; Suto, T.; Natal, M.-R.; Saddow, S. E.; Hatano, M.; Iwasaki, T., In situ bias current monitoring of nucleation for epitaxial diamonds on 3C-SiC/Si substrates. *Diamond and Related Materials* **2018,** *88*, 158-162.
4. Sumiya, H.; Toda, N.; Satoh, S., Development of high-quality large-size synthetic diamond crystals. *SEI TECHNICAL REVIEW-ENGLISH EDITION-* **2005,** *60*, 10.
5. Railkar, T. A.; Kang, W. P.; Windischmann, H.; Malshe, A. P.; Naseem, H. A.; Davidson, J. L.; Brown, W. D., A Critical Review of Chemical Vapor-Deposited (CVD) Diamond for Electronic Applications. *Critical Reviews in Solid State and Materials Sciences* **2000,** *25* (3), 163-277.
6. Butler, J. E.; Mankelevich, Y. A.; Cheesman, A.; Ma, J.; Ashfold, M. N., Understanding the chemical vapor deposition of diamond: recent progress. *J Phys Condens Matter* **2009,** *21* (36), 364201.
7. Nicley, S. S.; Nesládek, M.; Pobedinskas, P., Recent Advances in Diamond Science and Technology. *physica status solidi (a)* **2016,** *213* (10), 2550-2550.
8. Shenderova, O., *Detonation nanodiamonds: science and applications*. CRC Press: 2014.
9. Turcheniuk, K.; Mochalin, V. N., Biomedical applications of nanodiamond. *Nanotechnology* **2017,** *28* (25), 252001.
10. Schirhagl, R.; Chang, K.; Loretz, M.; Degen, C. L., Nitrogen-vacancy centers in diamond: nanoscale sensors for physics and biology. *Annual review of physical chemistry* **2014,** *65*, 83-105.
11. Dobrovitski, V.; Fuchs, G.; Falk, A.; Santori, C.; Awschalom, D., Quantum control over single spins in diamond. *Annu. Rev. Condens. Matter Phys.* **2013,** *4* (1), 23-50.
12. Childress, L.; Hanson, R., Diamond NV centers for quantum computing and quantum networks. *MRS bulletin* **2013,** *38* (2), 134-138.
13. Shikata, S., Single crystal diamond wafers for high power electronics. *Diamond and Related Materials* **2016,** *65*, 168-175.
14. Daeneke, T.; Khoshmanesh, K.; Mahmood, N.; De Castro, I.; Esrafilzadeh, D.; Barrow, S.; Dickey, M.; Kalantar-Zadeh, K., Liquid metals: fundamentals and applications in chemistry. *Chemical Society Reviews* **2018,** *47* (11), 4073-4111.
15. Fujita, J.-i.; Hiyama, T.; Hirukawa, A.; Kondo, T.; Nakamura, J.; Ito, S.-i.; Araki, R.; Ito, Y.; Takeguchi, M.; Pai, W. W., Near room temperature chemical vapor deposition of graphene with diluted methane and molten gallium catalyst. *Scientific Reports* **2017,** *7* (1), 12371.
16. Upham, D. C.; Agarwal, V.; Khechfe, A.; Snodgrass, Z. R.; Gordon, M. J.; Metiu, H.; McFarland, E. W., Catalytic molten metals for the direct conversion of methane to hydrogen and separable carbon. *Science* **2017,** *358* (6365), 917-921.
17. Chu, C.; d'Evelyn, M.; Hauge, R.; Margrave, J., Mechanism of diamond growth by chemical vapor deposition on diamond (100),(111), and (110) surfaces: Carbon-13 studies. *Journal of applied physics* **1991,** *70* (3), 1695-1705.

Acknowledgments:

We are grateful for the help of Seong-hun Lee, Seulyi Lee, and Hyun Jung Mun for their synchrotron X-ray experiments. **Funding:** This work was supported by IBS-R019-D1.